Cell Biol Toxicol (2025) 41:83
https://doi.org/10.1007/s10565-025-10037-3

RESEARCH

Activation of CaMKII$^+$ neurons in the paramedian raphe nucleus promotes general anesthesia in male mice

Xuehan Li · Zhixiong Ma · Xueliang Liu · Chen Chen · Ziqing Yu · Di Sang · Tongfei Wang · Eric Erquan Zhang · Guangyou Duan · Dapeng Ju · He Huang

Received: 11 November 2024 / Accepted: 24 April 2025

Abstract General anesthesia (GA) is an essential clinical and surgical adjunct, widely recognized as the result of coordinated networks among numerous brain regions. Anesthetic drugs with different characteristics are associated with distinct networks of brain regions involved in anesthesia. Ciprofol, a novel intravenous anesthetic derived from structural modifications of propofol, has shown promise in clinical applications. However, the specific neuronal circuits and brain regions mediating their actions may differ. Moreover, the core brain regions that mediate the common anesthetic effects of these drugs remain unclear. In this research, we identified a central ensemble of brainstem neurons within the paramedian raphe nucleus (PMnR) using c-Fos staining in mice subjected to GA induced by continuous intravenous infusion of ciprofol and propofol. This neuronal population, primarily composed of *CaMKIIa* and *Gad1*-expressing cells, demonstrated consistent activation in reaction to ciprofol. Optogenetic activation of PMnR^{CaMKIIa} neurons induced a GA state under ciprofol pre-administration, while sole activation of PMnR^{CaMKIIa} neurons induced a motionless state in mice. In addition, conditional inhibition of these neurons resulted in resistance to GA. In summary, we highlight the PMnR as a brain target for ciprofol and propofol. Furthermore, CaMKIIa$^+$ neurons in the PMnR emerge as active promoters of the anesthesia process, shedding light on a previously unrecognized key player in the intricate neural network orchestrating GA.

Keywords General anesthesia · Paramedian raphe nucleus · In situ sequencing · Optogenetics · Chemogenetic · Ciprofol · Propofol · Electroencephalogram

Supplementary Information The online version contains supplementary material available at https://doi.org/10.1007/s10565-025-10037-3.

X. Li · G. Duan · D. Ju (✉) · H. Huang (✉)
Department of Anesthesiology, The Second Affiliated Hospital, Chongqing Medical University, Chongqing, China
e-mail: judapeng@cqmu.edu.cn

H. Huang
e-mail: huanghe@cqmu.edu.cn

Z. Ma (✉) · T. Wang
Chinese Institute for Brain Research, Beijing, China
e-mail: mazhixiong@cibr.ac.cn

X. Liu
Department of Neurosurgery, Xinqiao Hospital, Third Military Medical University, Chongqing, China

C. Chen · Z. Yu · D. Sang · E. E. Zhang
National Institute of Biological Sciences, Beijing, China

E. E. Zhang
Tsinghua Institute of Multidisciplinary Biomedical Research, Tsinghua University, Beijing, China

Published online: 13 May 2025

Introduction

General anesthesia (GA) is a cornerstone in clinical surgical procedures, inducing an artificial physiological state characterized by unconsciousness, immobilization, analgesia, and amnesia (Arhem et al. 2003). While c-Fos staining has unveiled multiple neural nuclei implicated in promoting GA (Lanir-Azaria et al. 2018; Jiang-Xie et al. 2019; Gelegen et al. 2018; Nelson et al. 2002; Yi et al. 2023), our understanding of the specific target and circuit mechanisms underlying GA remains incomplete (Bastos et al. 2021). Current screening methods often rely on intersecting regions associated with various anesthetic mechanisms, including sleep-related ones (Zhang et al. 2022; Moody et al. 2021). Given that distinct drug mechanisms act on different brain regions (Tian et al. 2023; Wang et al. 2023), there is a need to identify the essential effects of anesthesia on brain regions activated by diverse anesthetic types.

Ciprofol, a novel intravenous anesthetic derived from structural modifications of propofol, designed to enhance the anesthetic experience by addressing some of the limitations associated with propofol (Qin et al. 2017). Recent studies have underscored that ciprofol outperforms propofol in several aspects, such as exerting less influence on breathing and blood circulation, having stronger efficacy, causing less pain during injection, and providing a larger safety range (Lu et al. 2023). While ciprofol and propofol exert their anesthetic effects primarily through interactions with the γ-aminobutyric acid subtype A ($GABA_A$) receptors, the specific neural circuits and brain regions mediating their actions may differ. For instance, ciprofol has a higher affinity for the $GABA_A$ receptor than propofol, which could influence its efficacy and safety profile (Qin et al. 2017; Liu et al. 2022). These results highlight the necessity for additional studies to clarify the precise neural pathways and key brain areas that underlie the fundamental anesthetic actions of these drugs.

In the present study, we employed intravenous injection for anesthesia induction, rapidly inducing mice into an anesthetic state mimicking clinical administration. Utilizing c-Fos staining, we systematically screened the entire brain for regions influenced by ciprofol and propofol (Liao et al. 2023). This unveiled the paramedian raphe nucleus (PMnR) in the brainstem as a previously unexplored region. Subsequent fiber photometry recordings confirmed PMnR neuron activation once it entered the GA state. Molecular characterization identified co-expression of both *CaMKIIa* and *Gad1* in PMnR c-Fos^+ neurons. Optogenetic activation increased δ wave power in electroencephalogram (EEG) and induced motionlessness, while inhibition resulted in resistance to transitioning into GA. Collectively, our results uncover a previously unrecognized yet crucial role of the PMnR in the ciprofol and propofol anesthesia process, thereby expanding the known neural substrates involved in the anesthetic network.

Method

Animals

Mice (3–5 animals per cage) were maintained separately in cages before experiments. The housing conditions were pathogen-free and maintained in a temperature-controlled setting of 22–24 °C and a relative humidity level of 38%−42% on a 12-h light/12-h dark cycle. All animals were given unrestricted access to food and water. To limit the impact of the circadian rhythm on the results, all experiments took place between Zeitgeber Time (ZT) 6 and ZT10. All procedures were carried out with the consent of the Institutional Animal Care and Use Committee (IACUC) at the National Institute of Biological Sciences in Beijing, adhering to the relevant regulations of the Chinese government. Adult male mice (8–10 weeks) were utilized. Wildtype C57/BL6 J mice were procured from Vital River and GemPharmatech. For targeted recombination in active populations, the Fos-Cre^{ERT2} mice (FosCre^{ER}, JAX#030323) (Guenthner et al. 2013) were on a B6.129 background and crossed with Ai6-zsGreen reporter mice ($R26^{Ai6}$, JAX#007906) (Madisen et al. 2010) to visualize the ciprofol/propofol-active neurons, second-generation of male FosCre$^{ER/+}$R26$^{Ai6/+}$ mice within the age range of 8 to 12 weeks were utilized for the experiments. Experiments involving optogenetic behavior began 3 to 4 weeks following the injection of adeno-associated virus, and were concluded within approximately 5 to 6 weeks. The mice were around 18 to 20 weeks old when all experiments were finished (Table 1).

Table 1 Key resources

Reagent or resource	Source	Identifier
Chemicals		
4-Hydroxytamoxifen(4-OHT)	MedChemExpress	Cat # HY-16950 A; CAS: 268,392–35-8
DAPI	MedChemExpress	Cat # D9542; CAS: 28,718–90-3
Deschloroclozapine (DCZ)	MedChemExpress	Cat # HY-42110; CAS: 1977–07-7
Ciprofol (2.5 mg/mL)	Haisco	HSK3486
Propofol (10 mg/mL)	Fresenius Kabi	J20171057
Ciprofol vehicle	Haisco	Batch Number: S20200301
Virus strains		
AAV2/9-mCaMKIIa-mCherry-WPRE-pA	Taitool	S0242-9
AAV2/9-hEF1a-DIO-mCherry-WPRE-pA	Taitool	S0197-9
AAV2/9-hVGAT-iCre-pA	Taitool	S0430-9
AAV2/9-hSyn-GCaMP6f-WPRE-pA	Taitool	S0536-9
pAAV-CaMKIIa-EGFP-P2 A-NLS-Cre-WPRE	Obiosh	CN870
rAAV2/9-EF1a-DIO-soul-mScarlet-WPRE-PA	Vector Core of CIBR (Chinese Institute for Brain Research)	BV02009(18)
AAV2/9-hEF1a-DIO-hM4D(Gi)-mCherry-ER2-WPRE-pA	Taitool	S0863-9
AAV2/9-mCaMKIIa-mCherry-WPRE-pA	Taitool	S0242-9
AAV2/9-hEF1a-DIO-mCherry-WPRE-pA	Taitool	S0197-9
Medications and medical devices		
Denture Base Materials	New century dental, China	20,173,170,702
Artifical Teeth Resin	New century dental, China	20,173,174,052
Erythromycin eye ointment (0.5%)	Chen xin, China	H37022025
Antibodies		
Rabbit monoclonal anti-c-Fos	Cell Signaling (CST)	Cat # 2250 s; RRID: AB_2247211
Donkey Anti-Rabbit IgG Antibody (Cy3®)	Jackson ImmunoResearch	Cat # 711–165-152; RRID: AB_2307443
Donkey Anti-Rabbit IgG HL (Alexa Fluor 488)	Abcam	Cat # ab150073; RRID: AB_2636877

Loss of righting reflex assay

Mice exhibiting loss of righting reflex (LORR) were unable to roll over onto all four limbs from a supine position. To assess their righting ability, they were taken out of the tail vein fixtation chamber and positioned on their back (Wasilczuk et al. 2018). Testing was conducted by an observer who knew which drug had been administered, and it was performed between ZT6 and ZT10.

Motionless assay

After laser stimulation, the timer started with the mouse holding a stationary position for 5 s until the mouse showed a combing motion or left the original position. If there was no continuous rest for 5 s, the timing was 0 s.

Surgical procedure

Mice were thoroughly anesthetized in a closed chamber filled with the inhalation anesthetic isoflurane (RWD, R510-22-10), and then fixed in a stereotaxic frame (RWD, Shenzhen, China); anesthesia was maintained with isoflurane inhalation (1%−2.5% via a tracheal). Their eyes were safeguarded using erythromycin ophthalmic ointment (0.5%). The skull was exposed and cleaned using 3% hydrogen peroxide. Then, two small holes in the skull above the PMnR were drilled at precise coordinates guided by the Mouse Brain in Stereotaxic Coordinates (George

Paxinos 2001). Viruses were injected into the PMnR (medial-lateral (ML) 0.25 mm, anterior–posterior (AP) −4.16 mm, and dorsal–ventral (DV) −4.3 mm) using a SMARTouch Controller (World Precision Instruments, Inc, Sarasota, Florida) injector at a speed of 46 nL/minute and 20 nL per side, bilaterally. An optical fiber (200 μm in diameter, N.A. =0.37) housed in a ceramic ferrule was positioned with its tip directly above the PMnR, outside the dura (Gong et al. 2020) (ML: 0.25 mm. AP: −4.16 mm.) in photogenetic activation test mice. Immediately after, mice in the photogenetic activation test and the chemogenetic inhibition test were equipped with three screw electrodes for EEG recording (2 frontal [1 mm frontal, 1 mm right-lateral from bregma] and 1 parietal [mid-distance below lambda] electrodes. Electromyogram (EMG) signals were detected directly from the neck muscle as previously described (Sang et al. 2023; Ma et al. 2022). Following the surgical procedure, mice were retained in a warm setting until they regained normal activity, as detailed earlier. Experiments were conducted for at least 21 days following surgery to ensure recovery and viral expression.

Fiber photometry

The AAV injection was administered first. Optical fiber implantation was then performed 30 min later. The ferrule containing an optical fiber (200 μm in diameter, N.A. =0.37) was fixed to the skull using dental cement, with the fiber tip positioned above the PMnR (coordinates: ML: 0.25 mm, AP: −4.16 mm, DV: −4.3 mm). The ferrule was secured on the skull with dental cement (Denture Base Material mixed with Artificial Teeth Resin at a 1:1 ratio). After the optical fiber was implanted, the skin was stitched, and erythromycin ophthalmic ointment (0.5%) was placed on the surgical incisions. Optogenetic stimulation and fiber photometry recording were carried out 3 weeks after the fiber implantation procedure to ensure recovery and viral expression.

Immunohistochemistry

Mice were thoroughly anesthetized using isoflurane and then underwent cardiac perfusion with 4% paraformaldehyde (PFA) in 1× Phosphate-Buffered Saline (PBS). Brain tissues were post-fixed for four to six hours in 4% PFA at ambient temperature and serially dehydrated using 30% sucrose in PBS. After freezing the brain at −15 °C for 10 min, coronal sections with a thickness of 20–30 μm were sliced using a cryostat microtome (CM1200, Leica). The brain sections were flushed using PBS (pH =7.4) and incubated with 5% normal donkey serum in PBS alongside 0.3% Triton X-100 for 2 h at ambient temperature. Primary antibodies used included rabbit anti-c-Fos (1:1000), were first incubated at 4 °C overnight, and then incubated with secondary antibodies (Donkey Anti-Rabbit IgG Antibody, 1:500, or Donkey Anti-Rabbit IgG HL, 1:1000) for 2 h at room temperature. Then, the brain sections were placed in Fluoromount-G (Millipore) and imaged using fluorescence microscopes (VS120 or VS200, Olympus). The quantity of c-Fos-labeled cells was evaluated utilizing a custom Image J script.

In situ sequencing (ISS)

For preparing brain sections, Optimal Cutting Temperature Compound (OCT)-embedded fresh mouse brain tissues were coronally sectioned into 10 μm thick slices using a cryostat. These slices were placed on glass slides and kept at −80 °C until needed. Adjacent two brain slices to the target region were retained for control and formal testing, respectively. The positive control genes *Ubc* and *Ppib* and the negative control gene *dapB* were selectively tested. Post-inspection, the slides were immersed in 4% PFA dissolved in phosphate-buffered saline treated with diethylpyrocarbonate (DEPC-PBS) at ambient temperature for 5 min, followed by rinses in DEPC-PBS twice. Subsequently, the slices were treated with 0.1 M hydrochloric acid (HCl) for 5 min and then rinsed in DEPC-PBS containing 0.05% Tween-20 (DEPC-PBS-T) for twice. Two sets of DNA ligation probes were developed targeting the genes under investigation. Excess probes were rinsed by DEPC-PBS-T and an additional imaging step was conducted before each round of sequencing to confirm the absence of residual signals. The ligation reaction was carried out in a mixture comprising 1× SplintR buffer (New England Biolabs), 10% glycerol, 0.2 μg/μL bovine serum albumin (BSA), 2.5 U/μL SplintR DNA ligase (New England Biolabs), and 1 U/μL RiboLock RNase Inhibitor (Thermo Fisher Scientific). The samples were incubated at 37 °C for 30

min and then washed with DEPC-PBS-T for three times. During the circularization process, 0.2 μM splint oligonucleotides were hybridized to dual-ligation probes in a solution containing 6× SSC and 10% formamide at room temperature for 30 min, simultaneously facilitating circularization and rolling-circle amplification (RCA). After being washed three times with DEPC-PBS-T, 1× Phi29 polymerase buffer (Thermo Fisher Scientific) and the corresponding detection probes was applied to the slides. These slides were dehydrated, placed in a Vectashield mounting medium (VectorLabs), and analyzed using an AxioplanII epifluorescence microscope (Zeiss). The imaging procedure utilized a 3D-Hitech Pannoramic® MIDI II system, which was configured with a pco.edge 4.2bi camera and a 20 ×objective lens. DAPI-stained images from one round were selected as the reference for subsequent analyses. The SIFI algorithm was employed to extract features from these DAPI images across multiple rounds. These extracted features were then matched across rounds, and the corresponding points were used to perform affine transformations to align the images. Background filtering was carried out using the tophat function from the OpenCV library. Finally, the spatial localization and quantification of RNA were validated by identifying and decoding authentic signals (Ke et al. 2013). RNA ISS Data analysis included image registration, correcting images, finding signal points, decoding signal points, and segmenting cells. The data analysis of RNA in situ sequencing was performed by Dynamic Biosystems (Suzhou, China). A gene-by-space matrix was generated and used in downstream analyses. DAPI images were used to detect nuclei using a Cellpose package (Stringer et al. 2021) for cellular segmentation. Then, each nucleus was expanded outwards until either a 20-pixel max distance was reached or the boundary of another cell was reached. Finally, a gene-by-cell matrix was generated. The PMnR region was delineated guided by the Mouse Brain in Stereotaxic Coordinates (George Paxinos 2001), with each cell encoded and the number of pixels in each cell counted based on the matrix. Every four pixels were recorded as one count, which was then used to calculate the expression intensity of each gene per cell.

Camk2a and Gad1 expression

The mixture of AAV2/9-hEF1a-DIO-mCherry-WPRE-pA with AAV2/9-hVGAT-iCre-pA (1:1) or CaMKIIa-mCherry was injected into the PMnR (20 nL per side, bilaterally). Three to four weeks later, mice underwent Anesthesia Process 1 followed by c-Fos immunohistochemistry.

Confocal microscopy

A confocal laser-scanning system attached to a Ti-E inverted microscope was used to capture the image stacks. The system was equipped with a 0.45 NA CFI Super Plan Fluor ELWD 20XC Nikon objective lens and operated using NIS-Elements AR 4.3 software. Excitation was provided by an argon ion laser (457–514 nm, 40 mW), a yellow DPSS laser (561 nm, 20 mW), a violet diode laser (405 nm, 50 mW), and a diode laser system (647 nm, 100 mW), each equipped with suitable filters. The z-stack images were taken with a spacing of 3 μm between each slice. The orientation of each section plane was determined with reference to the Mouse Brain in Stereotaxic Coordinates (George Paxinos 2001). Pseudo-coloring was applied in Image J during later processing stages where necessary.

Photogenetic activation and optical parameter verification

The optogenetic activator rAAV2/9-EF1a-DIO-soul-mScarlet-WPRE-PA with pAAV-CaMKIIa-EGFP-P2 A-NLS-Cre-WPRE or CaMKIIa-mCherry was expressed in the PMnR. Three to four weeks later, mice were anesthetized using ciprofol after an initial 5 min of baseline recording, and 70 to 100 s later, a laser of 473 nm (Fiblaser Technology, China) at 1 Hz lasting for 1 s was administered for 60 s to induce optical activation with an intensity of 30–40 mW (Zhou et al. 2023). For the feature of step-function opsin with ultra-high light sensitivity (SOUL) (rAAV2/9-EF1a-DIO-soul-mScarlet-WPRE-PA) (Gong et al. 2020), laser off was not meant to functionally opsin off. The anesthetic dose was established at the anesthesia concentration at which 50% of the population would not enter a state of anesthesia. For the subsequent analysis, selection was limited to mice that successfully received drug injections on their first try.

The duration of LORR in mice was measured without any additional stimulation. Additionally,

mice were re-anesthetized for the procedure to test the response to noxious stimuli at least one week later. Gentle pressure was applied to the terminal end of the mouse's tail, and the absence of a return of the righting reflex (RORR) was observed as a sign that the mouse was in a GA state.

Chemogenetic inhibition

The chemogenetic inhibitor AAV2/9-hEF1a-DIO-hM4D(Gi)-mCherry-ER2-WPRE-pA mixed with pAAV-CaMKIIa-EGFP-P2 A-NLS-Cre-WPRE was expressed in the PMnR (20 nL per side, bilaterally). DCZ treatment: DCZ (HY-42110, MedChemExpress) was prepared by dissolving it in 1–2% dimethyl sulfoxide (DMSO) in saline, resulting in a final volume of 0.1 mL/kg (1 mg/kg), each mouse intraperitoneal injection of 1 mg/kg and back to the cage 30 min before the experiment. The saline treatment was given 0.1 mL/kg of saline injected intraperitoneally and back to the cage 30 min before the experiment. All animals received two types of treatments, and the experimental interval was at least one week.

EEG/EMG process

EEG/EMG signals underwent amplification and filtering (0.5–35 Hz for EEG; 100–500 Hz for EMG) and digitized at 2000 Hz by signal conditioners (EEG 100 C and EMG 100 C amplifiers-Biopac MP160) (BIOPAC Systems, Inc). The signals were captured using AcqKnowledge software (version 5.0, Biopac Systems) at a sample rate of 2000 Hz and saved for offline analyses. Power spectrum density was calculated by EEGlab (Delorme and Makeig 2004), and the time-frequency spectrogram was visualized by multitaper spectrogram (Prerau et al. 2017). The limit frequencies range from 0 to 35 Hz. The time bandwidth is 15 s, and the number of tapers is 30. The Window size is 30 s, with a step size of 5 s. The data was not detrended or smoothed. Power for every frequency range from 0 to 35 was added as the total power, and the total sum of specific band ranges (delta [δ 0–4 Hz], theta [θ 4–8 Hz], alpha [α 8–12 Hz], and beta [β 13–30 Hz]) was divided to the total power.

Anesthesia process

1. c-Fos staining for whole brain screen and co-expression with Camk2a or Gad1: the mice were domesticated under 12L:12D conditions for one week, and the drugs were treated at ZT6-ZT10. Connect the infusion needle to the injection needle, fill it with propofol/ciprofol, and leave it at ambient temperature for 10 min. Experimental group: mice were placed in a tail vein fixator tube, and a relatively thick and straight side of the tail vein was found. Alcohol cotton balls were applied to the root of the mouse tail to the injection point and intravenous injection of 10 to 12 mg/kg propofol or 4 to 5 mg/kg of ciprofol. The infusion needle was fixed with adhesive tape, and the mice were removed from the tube and positioned on a cushion. The infusion rate was maintained at 0.3 mL/h to 0.4 mL/h (Syringe Pump, LPS02-2 A), and the respiratory rate of the mice was controlled at 80–130 times/min. Stop the medication after 2 h and euthanize the mice. Untreated control group: euthanized at the same time point as the experimental group.
2. Genetic capture of propofol/ciprofol labeled neurons using Fos-Cre$^{ER/+}$R26$^{Ai6/+}$ mice: FosCre$^{ER/+}$R26$^{Ai6/+}$ mice domesticated under 12L:12D conditions for one week, and the drugs were treated at ZT6-ZT10. Propofol/ciprofol overlay test: The schedule of drug treatment was the same as mentioned above in Anesthesia Process 1 and intraperitoneally injected with 50 mg/kg 4-OHT which was used for CreERT2 recombination in active cells. This process leads to the transcription and translation of fluorescent proteins, thereby causing the activated cells to express zsGreen fluorescent proteins in Fos-Cre$^{ER/+}$R26$^{Ai6/+}$ mice (Guenthner et al. 2013). One week later, the above process was repeated with the other drug, and mice were euthanized for c-Fos immunofluorescence analysis. Ciprofol specificity test: Experimental group: mice were intravenously injected with 10 mg/kg (4 mL/kg) of ciprofol to ensure a long enough LORR duration to visualize c-Fos. Vehicle control group: intravenous injection of equal-dose volume (4 mL/kg) of ciprofol vehicle. Two groups of mice

were given 50 mg/kg 4-OHT via intraperitoneal injection.

3. Fiber photometry recording: mice were intravenously injected with ciprofol vehicle (2–4 mL/kg) for an initial 5 min of baseline recording, and 10 min later received an intravenous injection of 5–10 mg/kg (2–4 mL/kg) of ciprofol to ensure that all mice enter an anesthetic state.
4. Exploration of Effect-Dose (ED) curve of ciprofol: mice were placed in a tail vein fixation chamber and loaded onto the tail vein injector, and the relatively thick and straight portion of the tail vein was identified. The tail root of the mouse was gently rubbed with an alcohol-soaked cotton ball to prepare the injection site. Intravenous injections of ciprofol were administered at various doses (1.25, 2.5, 3, 3.125, 3.25, 3.75, 4.25, and 6 mg/kg) ($n = 10$). After injection, the mouse was removed from the chamber and placed in a supine position. The rate of LORR was calculated for each dose. All experiments were conducted between ZT6 and ZT10, with a one-week interval between each dose administration. For the subsequent analysis, selection was limited to mice that successfully received drug injections on their first try.

Statistical analysis

Data processing and analysis were conducted using Excel and GraphPad Prism 9. Statistical methods employed included unpaired and paired t-tests, one-way ANOVA with parametric tests and Tukey's multiple comparisons, one-way ANOVA with Dunn's test or the Benjamini-Krieger-Yekutieli correction for multiple comparisons, and two-way ANOVA with Holm-Sidak correction as needed. Nonlinear regression analysis using a Log (Agonist) *vs*. Response model was employed to fit the Effect-Dose curve. Unless specified otherwise, data are shown as mean ± SEM, with the n value indicated for each dataset. Significant results are detailed in the figure legends. The significance level was set at 0.05, two-tailed (not significant, ns; $p > 0.05$; * $p < 0.05$; ** $p < 0.01$; *** $p < 0.001$; **** $p < 0.0001$). Mice from different litters were assigned to various treatment groups at random, with no further specific randomization techniques used in the animal experiments.

Results

PMnR in the brainstem is commonly activated in GA state by propofol and ciprofol

To comprehensively investigate the brain regions activated during anesthesia, we conducted a whole-brain screen using c-Fos, which was visualized after 2 h of anesthesia with ciprofol or propofol in C57BL/6 J mice (Fig. S1A). Strikingly, both ciprofol and propofol selectively activated the PMnR, as evidenced by pronounced c-Fos expression (Fig. 1A-E). Additionally, previously identified responsive brain regions, such as lateral preoptic area (LPO) (Gordon-Fennell et al. 2019), lateral habenula (LHb) (Gelegen et al. 2018), supraoptic nucleus (SON) (Jiang-Xie et al. 2019), and Edinger-Westphal nucleus (EW) (Yi et al. 2023), exhibited notable c-Fos expression during treatment with either ciprofol or propofol (Fig. S1B-S1F). Notably, SON was not activated by ciprofol, while the c-Fos$^+$ cell in LHb showed a statistically significant difference between ciprofol and propofol treatment (Fig. S1G).

For real-time recording of PMnR neuronal activity during the GA state, we employed photometry recording during ciprofol administration. C57BL/6 J mice were injected with hSyn-GCaMP6f virus in the PMnR region (Fig. 1F). Real-time fiber photometry assay was used to detect the Ca^{2+} activities of PMnR neurons (Fig. 1G). The results revealed an immediate increase in Ca^{2+} activities upon ciprofol-induced LORR (Wasilczuk et al. 2018), coinciding with the mice entering the GA state (Fig. 1H).

To further confirm the results, Fos-Cre$^{ER/+}$R26$^{Ai6/+}$ mice (Guenthner et al. 2013) sequentially treated with the two drugs and labeled for c-Fos expression in green and magenta colors separately (Fig. S2A), the results demonstrated a similar pattern of PMnR neuron activation for the two anesthetics (Fig. S2B-S2G). Notably, ciprofol triggered a higher proportion of activated neurons than propofol whether in propofol-ciprofol order (ciprofol ratio: 64.29% ± 2.72%; propofol ratio: 51.31% ± 1.65%) or reversed order (ciprofol ratio: 58.74% ± 3.86%; propofol ratio: 40.85% ± 3.42%). Consequently, ciprofol was prioritized for subsequent experiments to detect and modulate neurons in the PMnR brain area.

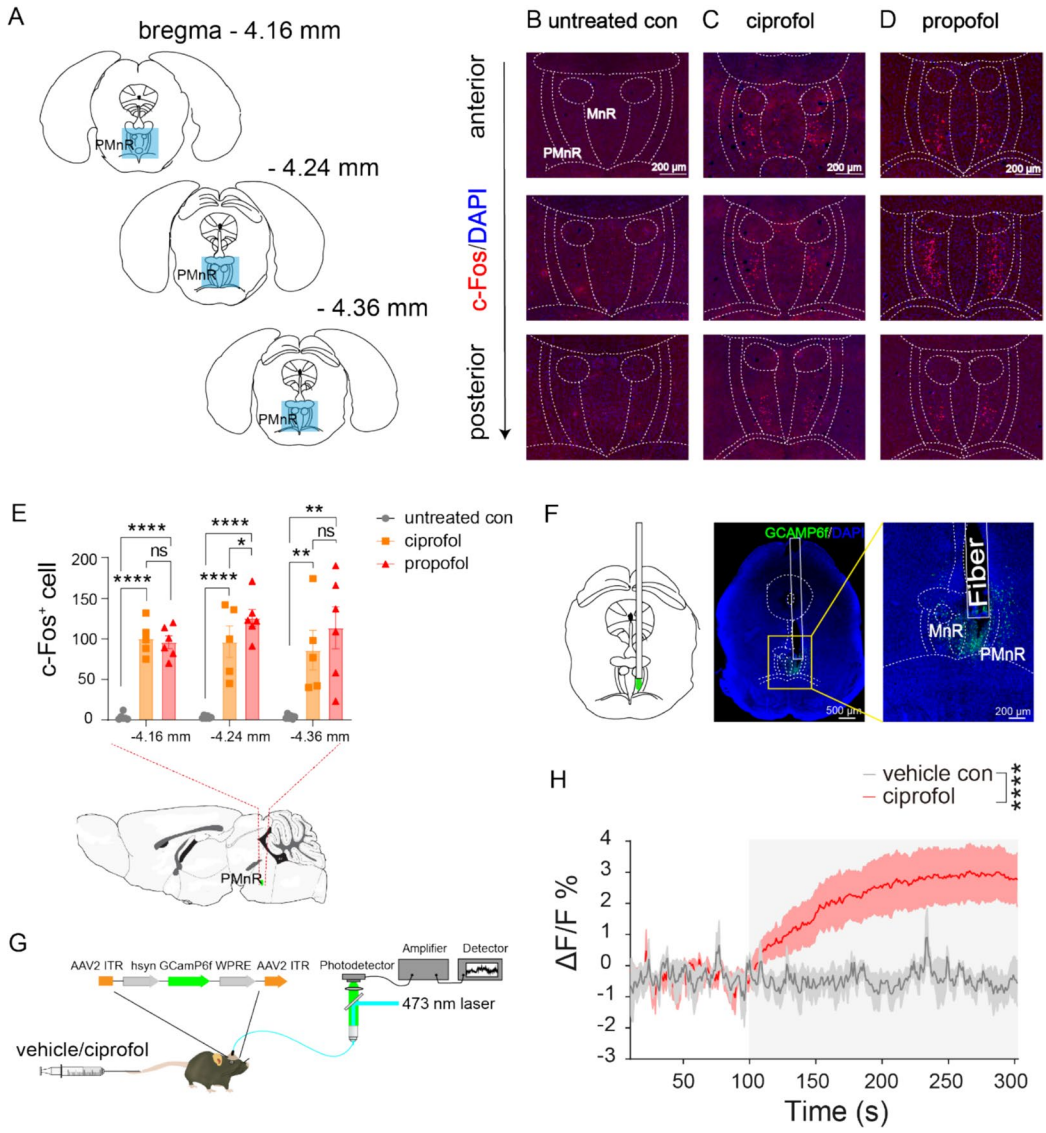

Fig. 1 Neurons were activated by anesthesia unconsciousness state, specifically in PMnR. **A** Schematic of associated regions on the brain atlas. **B-D** Representative labeled c-Fos^{+} cells (Arrow direction: approximately −4.16 mm to −4.36 mm from bregma) after 2 h of continuous intravenous ciprofol/propofol injection from $n = 5$ to 6 mice are shown. **E** The graph shows the number of c-Fos labeled neurons across the PMnR region for mice ($n = 3$ sections from 6 mice in the control group and propofol group, 5 mice in the ciprofol group). (−4.16 mm slice: F (2, 14) = 63.86, $p < 0.0001$; −4.24 mm slice: F (2, 14) = 30.80, $p < 0.0001$; −4.36 mm slice: F (2, 14) = 8.414, $p = 0.0040$). See also Figure S1G. **F** Representative coronal section of WT mice depicting the injection site of AAV-hsyn-GCAMP6f (green) and DAPI (blue) in the PMnR. **G** Experimental strategy for fiber optic implantation and device connection. **H** Normalized GCaMP fluorescence changes (green, ΔF/F) in PMnR neurons alongside the time course of vehicle (gray) and ciprofol (red) injection; the injection time point was at 100 s ($n = 6$). Statistical analysis was performed using ordinary one-way ANOVA tests in E with a two-stage linear step-up procedure of Benjamini, Krieger, and Yekutieli correction, and the two-way ANOVA with Holm-Sidak correction test in H. Data is presented as mean ± SEM. *$p < 0.05$, **$p < 0.01$, ***$p < 0.001$, ****$p < 0.0001$, ns $p > 0.05$. Con, control. See also Figures S1 and S2

To exclude noise induced by the vehicle, an equal-dose volume vehicle was injected into Fos-Cre$^{ER/+}$R26$^{Ai6/+}$ mice (Fig. S2H, S2I). The dosage was set according to LORR duration induced by signal drug injection that satisfied the c-Fos expression requirement of Fos-Cre$^{ER/+}$R26$^{Ai6/+}$ mice (Guenthner et al. 2013) (Fig. S2H), while the dose of propofol to reach this duration often causes severe respiratory suppression or even death. c-Fos expression was rarely observed in PMnR, confirming the specific activation of PMnR neurons by GA state rather than procedural effects (Fig. S2J, S2K).

Ciprofol-activated PMnR neurons predominantly exhibit CaMKIIa$^+$ expression

To discern the specific subtype of neurons responsive to ciprofol and propofol administration, we employed an integrated Fos-Cre$^{ER/+}$R26$^{Ai6/+}$ mice (Guenthner et al. 2013) and an in situ sequencing (ISS) (Ke et al. 2013) strategy to screen for neuronal markers in the PMnR. To distinguish neuron type through neurotransmitters in neurons, the following candidate markers, including *Camk2a*, *Gad1*, *Slc17a6*, *Slc17a8*, and *Tph2*, were examined, with *NeuN* serving as the neuron marker (Fig. 2A). Cellpose package was used to predict the cell outline (Stringer et al. 2021). Our results revealed that most (93.33%) of c-Fos-targeted cells expressed the neuron marker *NeuN* (Fig. 2B). Among the candidate markers, *Gad1* (encoding glutamate decarboxylase 1, Gad1) and *Camk2a* (encoding calcium/calmodulin-dependent protein kinase II alpha, CaMKIIa) exhibited a substantially higher ratio of c-Fos-targeted cells (86.66%), indicating that the c-Fos-targeted neurons highly express both *Camk2a* and *Gad1* (Fig. 2B). Other makers, such as *Tph2*, *Slc17a6,* and *Slc17a8* (Fig. 2B, C), exhibited less abundant expressed mRNA reads.

To validate whether the Gad1 and CaMKIIa are highly expressed in neurons by ISS, immunostaining of c-Fos and specific gene promoter driver mCherry expression were performed (Fig. 2D). Given expression patterns of Gad1 and vesicular GABA transporter (VGAT) are highly correlated and often used as markers for GABAergic neurons, CaMKIIa-mCherry and hVGAT-mCherry (combination of AAV2/9-hEF1a-DIO-mCherry-WPRE-pA and AAV2/9-hVGAT-iCre-pA, 1:1) were injected into the PMnR, induced with ciprofol, and subsequently underwent immunofluorescence staining of c-Fos. The results demonstrated a significant overlap between CaMKIIa$^+$/VGAT$^+$ and c-Fos$^+$ cells (Fig. 2E, F). No difference was found between the CaMKIIa$^+$ and VGAT$^+$ group for the probability of c-Fos expression (CaMKIIa$^+$c-Fos$^+$/c-Fos$^+$: 89.60% ±3.16%; VGAT$^+$c-Fos$^+$)/c-Fos$^+$: 90.71% ±2.73%, Fig. 2G). Given the features of PMnR (Sos et al. 2017), our findings indicate that ciprofol and propofol-activated neurons expressed multiple gene markers.

CaMKIIa$^+$ neurons activation in PMnR promotes transition to light anesthesia

To delve into the relationship between the neural dynamics of PMnR neurons and the anesthesia state, we employed optogenetic activation of this brain region under pre-administration of ciprofol 3 mg/kg, the ED50 concentration. DIO-SOUL (Gong et al. 2020) with *Camk2a* promoter-driven Cre recombinase virus or CaMKIIa-mCherry virus was injected into the PMnR (Fig. 3A). Simultaneously, EEG recording was applied to detect the activation effect of neurons during the opto-activation procedure in the PMnR.

After three to four weeks, mice received an intravenous injection of ciprofol (3 mg/kg), and the mice who did not exhibit the loss of the righting reflex (unLORR) transitioned into light GA state underwent 473 nm laser opto-stimulation to activate neurons in the PMnR (Figs. S3 and 3B). The behavioral results also demonstrated that the activation of PMnR^{CaMKIIa} neurons markedly induced the transition of mice from a wake to a LORR state (Video 1.1 of Con mice and Video 1.2 of SOUL mice). And the mice were unawakened by noxious stimulation (Video 1.3). Muscle activity was substantially suppressed (Fig. 3C), and LORR duration was substantially induced by the activation of PMnR^{CaMKIIa} neurons (Fig. 3D, t = 7.2510, *df* = 8). In addition, EEG recordings from the cortex in mice suggested a prominent interaction between optical PMnR^{CaMKIIa} neuron activation and the low-frequency band (Fig. 3C, E and F). Utilizing EEG brain wave range division standards (delta [δ 0–4 Hz], theta [θ 4–8 Hz], alpha [α 8–12 Hz], and beta [β 13–30 Hz]), power spectral density (PSD) ratio analysis of the EEG signal suggested PMnR activation greatly increased in δ band (Fig. 3G and H, PSD ratio$^{unLORR\ phase}$ = 0.25 ±0.04,

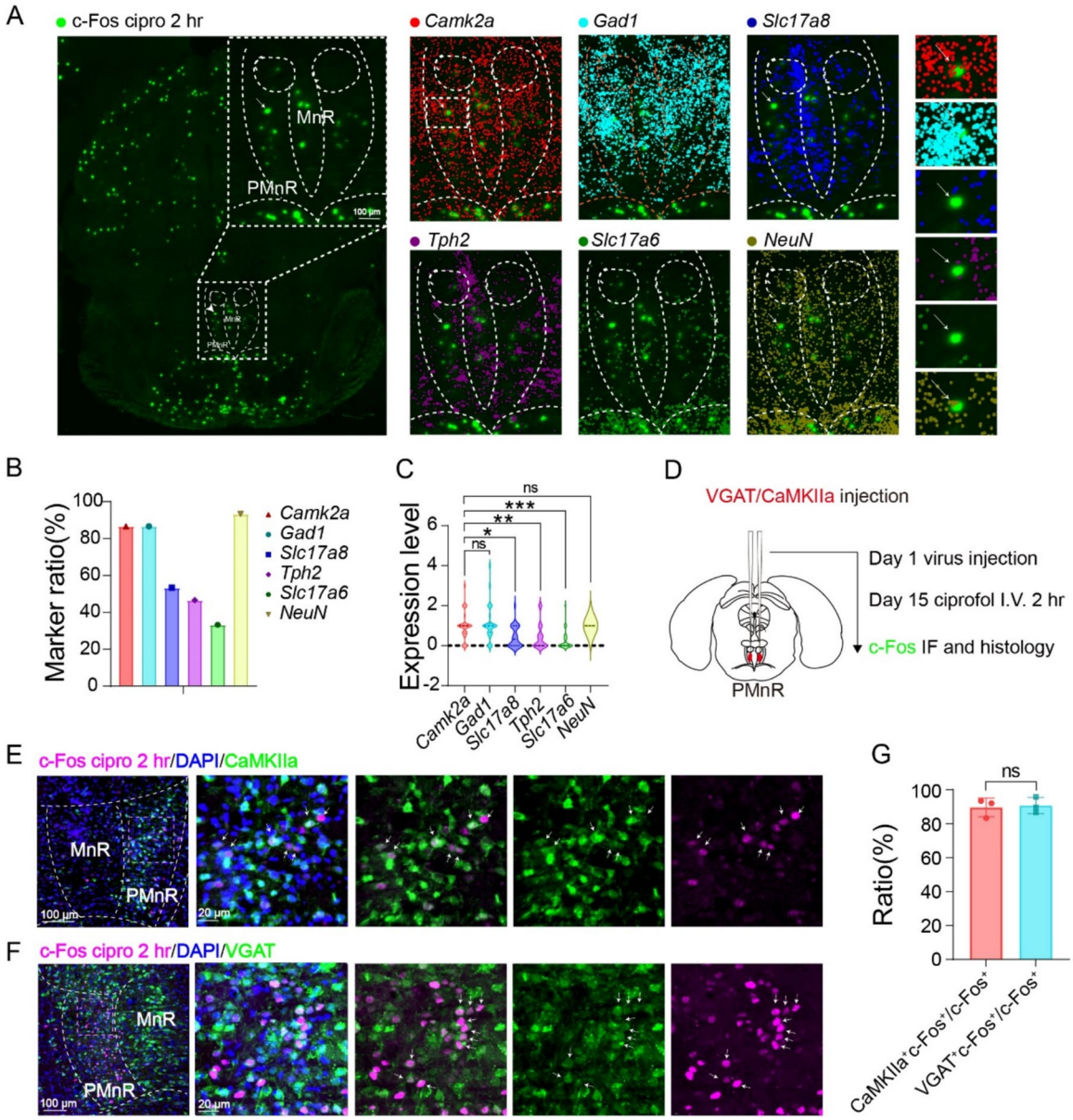

Fig. 2 Molecular signatures of c-Fos$^+$ neurons throughout the PMnR. **A** Co-labeled candidate genes (*Camk2a*, *Gad1*, *Slc17a8*, *Tph2*, *Slc17a6*, and *NeuN*) with c-Fos (green) labeled neurons induced by ciprofol in PMnR. Arrow, c-Fos labeled neurons. **B** Histogram chart of the ratio for candidate genes over c-Fos labeled cells. **C** Violin Chart depicting the normalized expression level of *Camk2a*, *Gad1*, *Slc17a8*, *Tph2*, *Slc17a6*, and *NeuN*. **D** Virus injection and experimental strategy flowchart. **E–F** Representative image of c-Fos-labeled neuron (Magenta) induced by ciprofol in CaMKIIa-mCherry (green) and VGAT-mCherry (green) expressing cells in PMnR. Arrow, c-Fos-marked neurons. **G** Histogram of the ratio for double-labeled CaMKIIa$^+$c-Fos$^+$ and VGAT$^+$c-Fos$^+$ neurons over the c-Fos$^+$ cell ($n = 3$, respectively). Statistical analysis was performed using one-way ANOVA by Dunn's multiple comparisons test in C, and unpaired *t*-test (parametric) in G. Data are presented as mean ± SEM. $^*p < 0.05$, $^{**}p < 0.01$, $^{***}p < 0.001$, ns $p > 0.05$

PSD ratio$^{\text{laser phase}}$ = 0.40 ±0.02, mean ±SEM, p < 0.05), while greatly decreased in β band (Fig. 3G and H, PSD ratio$^{\text{unLORR phase}}$ = 0.38 ±0.03, PSD ratio$^{\text{laser phase}}$ = 0.21 ±0.01, mean ±SEM, p < 0.05). These data was in consistent with the normalized ΔPSD ratio (Fig. 3I). The results demonstrated that the activation of PMnR$^{\text{CaMKIIa}}$ neurons markedly promotes the transition from wakefulness to GA.

To explore the neural dynamics of PMnR neurons corresponding to the behavior of mice, a 473 nm laser opto-stimulation was applied to activate neurons in the PMnR without ciprofol injection (Fig. S4A, S4B). The results reveal that the activation of PMnR$^{\text{CaMKIIa}}$ neurons induced the mice to stand motionlessly (Video 2.1 of Con mice and Video 2.2 of SOUL mice), and motionless duration was greatly induced by the activation of PMnR$^{\text{CaMKIIa}}$ neurons (Fig. S4C, S4D). Muscle activity was suppressed, notably, supporting the behavioral changes, which was more than a sedation state showing no locomotor speed or distance during the motionless duration (Gelegen et al. 2018; Xu et al. 2022). Activation of PMnR$^{\text{CaMKIIa}}$ induced EEG δ wave accumulation compared with control group during the motionless phase (Fig. S4C, S4F-S4H, PSD ratio$^{\text{baseline}}$ = 0.42 ±0.02, PSD ratio$^{\text{laser phase}}$ = 0.52 ±0.02, mean ±SEM, p < 0.05, t_{δ} = 3.8830, df =4), which were in consistent with previous data. Meanwhile, it also induced decrease in α and β wave bands (Fig. S4G, S4H). These data were in consistent with the normalized ΔPSD ratio (Fig. S4I, p = 0.0051, t_{δ} = 3.8180, df = 8). Following the experiment, brain sections were prepared, and the injection site of the virus was examined (Fig. S5). In summary, activation of PMnR$^{\text{CaMKIIa}}$ neurons without ciprofol pre-administration also approaches GA, as demonstrated in EEG and EMG.

In summary, the data showed activation of this brain region increased the PSD ratio of the δ band wave and decreased the β band. Behaviorally, the activation of PMnR$^{\text{CaMKIIa}}$ neurons significantly facilitated the induction of mice transitioning from a waking state towards a loss-of-consciousness state.

Chemogenetic inhibition of CaMKIIa^{+} neurons in PMnR induces resistance to LORR

To further investigate how the CaMKIIa^{+} neurons in PMnR operate in the LORR, we sought to examine the inhibitory effect of PMnR neurons. We employed a chemogenetic inhibition method. DIO-hM4Di with CaMKIIa-driven Cre recombinase virus or CaMKIIa-mCherry was injected into the PMnR region (Fig. 4A). EEG recording was also performed to monitor the brain wave (Fig. 4B). Three to four weeks later, the same volume of DCZ (1 mg/kg) (Nagai et al. 2020) or saline was administered intraperitoneally 30 min before ciprofol administration (Fig. 4C). A camera recorded behavioral performance to determine the LORR rate. As anticipated, inhibiting PMnR$^{\text{CaMKIIa}}$ neurons dramatically reduced the LORR rate compared to saline treatment (Fig. 4D, DCZ: 0%; saline: 100%, p < 0.01, n = 5) (Video 3.1 hM4Di mice of saline and Video 3.2 hM4Di mice of DCZ). This result highlights that the early inhibition of PMnR neurons leads to resistance in transitioning into the LORR state (Fig. 4D). We further observed the EEG pattern which was applied by the chemogenetic inhibition of PMnR$^{\text{CaMKIIa}}$ neurons (Fig. 4E). Conversely, a decreased θ PSD ratio and an increased β PSD ratio were seen in the chemogenetic inhibition of CaMKIIa^{+} neurons in the PMnR (Fig. 4F and G). In comparison, the other bands (δ and α bands) showed no significant difference (Fig. 4G, t_{δ} = 1.9680, df = 4; t_{θ} = 2.5070, df = 4; t_{α} = 1.3550, df = 4; t_{β} = 3.6050, df = 4). The mice were only included with correct injection sites, and the EEG and EMG curves were clear (Fig. S6A). Besides, the control group mice consistently demonstrated similar behavioral performance and EEG patterns, regardless of whether they received saline or DCZ injections. (Figs. 4D, S6B, and S6C).

In summary, the data showed that this brain region is inhibited during anesthesia by decreasing the power density of the θ band wave. Behaviorally, the inhibition of PMnR$^{\text{CaMKIIa}}$ neurons significantly attenuated the induction of mice transitioning from a waking state to the LORR state.

Discussion

Given that c-Fos responds to sharp and rapid stimulation (Hagihara et al. 2021), we employed tail vein administration, ensuring a swift transition into the GA state, in contrast to intraperitoneal injection (Wasilczuk et al. 2018). Through c-Fos staining for whole-brain screening, we initially identified the PMnR as a novel brain region activated by ciprofol and propofol treatment (Figs. 1 and S1). Intriguingly, our investigation also

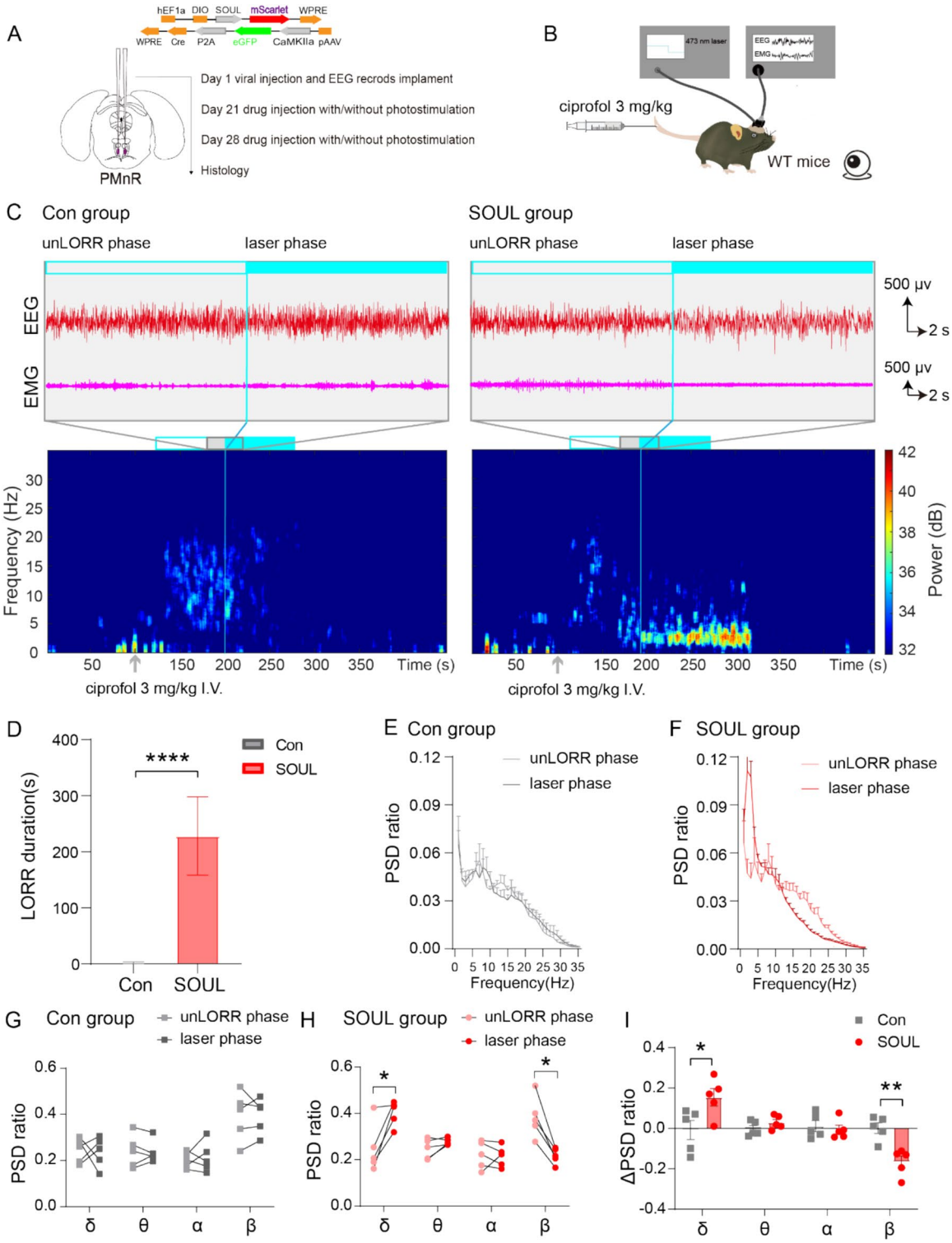
A
hEF1a DIO SOUL mScarlet WPRE
WPRE Cre P2A eGFP CaMKIIa pAAV
Day 1 viral injection and EEG recrods implament
Day 21 drug injection with/without photostimulation
Day 28 drug injection with/without photostimulation
Histology
PMnR
B
473 nm laser
EEG
EMG
ciprofol 3 mg/kg
WT mice
C Con group
SOUL group
unLORR phase
laser phase
EEG
EMG
500 μv
2 s
Frequency (Hz)
Power (dB)
Time (s)
ciprofol 3 mg/kg I.V.
D
LORR duration(s)
****
Con
SOUL
E Con group
F SOUL group
PSD ratio
Frequency(Hz)
G Con group
H SOUL group
δ
θ
α
β
I
ΔPSD ratio
*
**

◂**Fig. 3** Optogenetic activation of CaMKIIa^{+} neurons in the PMnR induced LORR and δ wave band. **A** Viral-genetic approach for the expression of SOUL in PMnR^{CaMKIIa} neurons. **B** The layout of optic fiber implantation and EEG/EMG recording, and mice will receive 3 mg/kg ciprofol injection tail intravenously and 473 nm laser stimulation. **C** Upper left: representative traces of EEG and EMG of the phase 20 s before and after laser stimulation corresponding to the lower part of the control group. Lower left: time-frequency spectrogram of EEG of 100 s before ciprofol injection and 350 s after laser. Upper right: representative traces of EEG and EMG of the phase 20 s before and after laser stimulation corresponding to the lower part of the SOUL group. Lower right: time-frequency spectrogram of EEG of 100 s before ciprofol injection and 350 s after laser. The laser stimulation schedule is 1 Hz, lasting for 1 s, 30–40 mW, for 60 s. Period included in data analysis: unLORR phase: from ciprofol injected timepoint to laser (100 s to 200 s); laser phase: from 473 nm laser stimulation to RORR (200 s to RORR). **D** LORR duration of the SOUL injected mice was induced by laser stimulation compared to the control group. (unpaired *t*-test: $t = 7.2510$, $df = 8$). **E** 473 nm laser shows no effect on the normalized global EEG wavelet PSD ratio from control mice corresponding to (C) ($n = 5$). **F** 473 nm laser-induced changes in the normalized global EEG wavelet PSD ratio from SOUL mice ($n = 5$). **G** PSD ratio of δ/θ/α/β band before and after the optical activation in the control group corresponding to (E). (paired *t*-test: $t_{\delta} = 0.1680$, $df = 4$; $t_{\theta} = 0.1344$, $df = 4$; $t_{\alpha} = 0.4200$, $df = 4$; $t_{\beta} = 0.0521$, $df = 4$). **H** PSD ratio of δ/θ/α/β band before and after the optical activation in the SOUL group corresponding to (F). (paired *t*-test: $t_{\delta} = 3.625$, $df = 4$; $t_{\theta} = 1.933$, $df = 4$; $t_{\alpha} = 0.2596$, $df = 4$; $t_{\beta} = 5.7030$, $df = 4$). **I** Alterations in the δ/θ/α/β PSD ratio in control and SOUL group after laser. (unpaired *t*-test: $t_{\Delta\delta} = 2.5530$, $df = 4$; $t_{\Delta\theta} = 1.424$, $df = 4$; $t_{\Delta\alpha} = 0.4901$, $df = 4$; $t_{\Delta\beta} = 4.2770$, $df = 4$). Three periods that interfere with the EEG were removed when processing data: 1. the unstable period of recording EEG at the beginning; 2. the period of mice equipped with tail vein injection equipment; 3. the initial unstable period of light activation. Also applicable to Fig. S3. Statistical analysis was performed using a paired *t*-test (parametric) in G and H, and an unpaired *t*-test (parametric) in D and I, Data are presented as mean ± SEM. $*p < 0.05$, $**p < 0.01$, $***p < 0.001$, ns $p > 0.05$. See also Figures S3, S4, and S5. See also Video 1.1 and Video 1.2

implicated other areas previously reported to play a positive role in promoting GA function (Fig. S1) (Jiang-Xie et al. 2019; Gelegen et al. 2018). Some regions that are not involved in ciprofol but are involved in propofol also play an essential role in promoting general anesthesia (GA), such as SON (Jiang-Xie et al. 2019) (Fig. S1G). The lack of involvement of the SON underscores the distinct characteristics of the two drugs, which merit further exploration.

The identification of the PMnR as a crucial node governing arousal and motor brainstem nuclei, as reported in human fMRI studies (Singh et al. 2022), aligns with its established role in behavioral phenotypes associated with arousal and motor functions (Leiras et al. 2022; Caggiano et al. 2018; Wang et al. 2021; Ao et al. 2021). Notably, previous studies in mice have not dissected the specific functions of the PMnR from the broader medial raphe (MR) area, leaving its solitary behavioral role unclear (Sakurai et al. 2005; Hsu et al. 2013). Our work found that activation for the region led to a fast transition from waking toward the GA state, and inhibition of these neurons led to the mice dramatically reducing the LORR rate, which supports that the PMnR region works on inhibiting arousal and motor function. In our study, the Ca^{2+} activity of PMnR neurons increased precisely when mice entered the LORR state; this result indicates that PMnR was essential to the induction stage of general anesthesia. However, whether the PMnR region works on general anesthesia's maintenance or emergence stages warrants further investigation.

Previous studies employing in-situ hybridization have indicated high expression levels of vesicular GABA transporter (VGAT) in the PMnR region (Sos et al. 2017). In our study, an expression rate exceeding 50% for CaMKIIa and VGAT in PMnR c-Fos^{+} cells suggests that these two neuronal markers may coexist within the same cellular population (Fig. 2E, F, and G). While there are reports of neurons co-expressing markers of both excitatory and inhibitory neurotransmitter systems in specific brain regions (Root et al. 2018), the co-expression of CaMKIIa with GAD1 and VGAT in the same neurons is not a common occurrence. However, due to the limitations inherent in our study design, we could not establish the co-expression of these two markers within the same neurons. Future research will be needed to elucidate the precise molecular mechanisms of drug action in the PMnR.

The conventional understanding of GA in mice has centered on reduced movement and a shift in PSD from β or γ to θ and δ ranges in EEG (Jiang-Xie et al. 2019; Xia et al. 2023), which corresponds to a gradual deepening of anesthesia depth (Esteves et al. 2019). Additionally, θ waves (4–8 Hz) dominated the changes from baseline to unconsciousness during slow propofol induction, while δ waves (0.5–4 Hz) have been implicated in an advanced depth of anesthesia after LORR (Lee et al. 2017; Hagihira 2015, 2017; Lin et al. 2023). Also, we proved that the θ

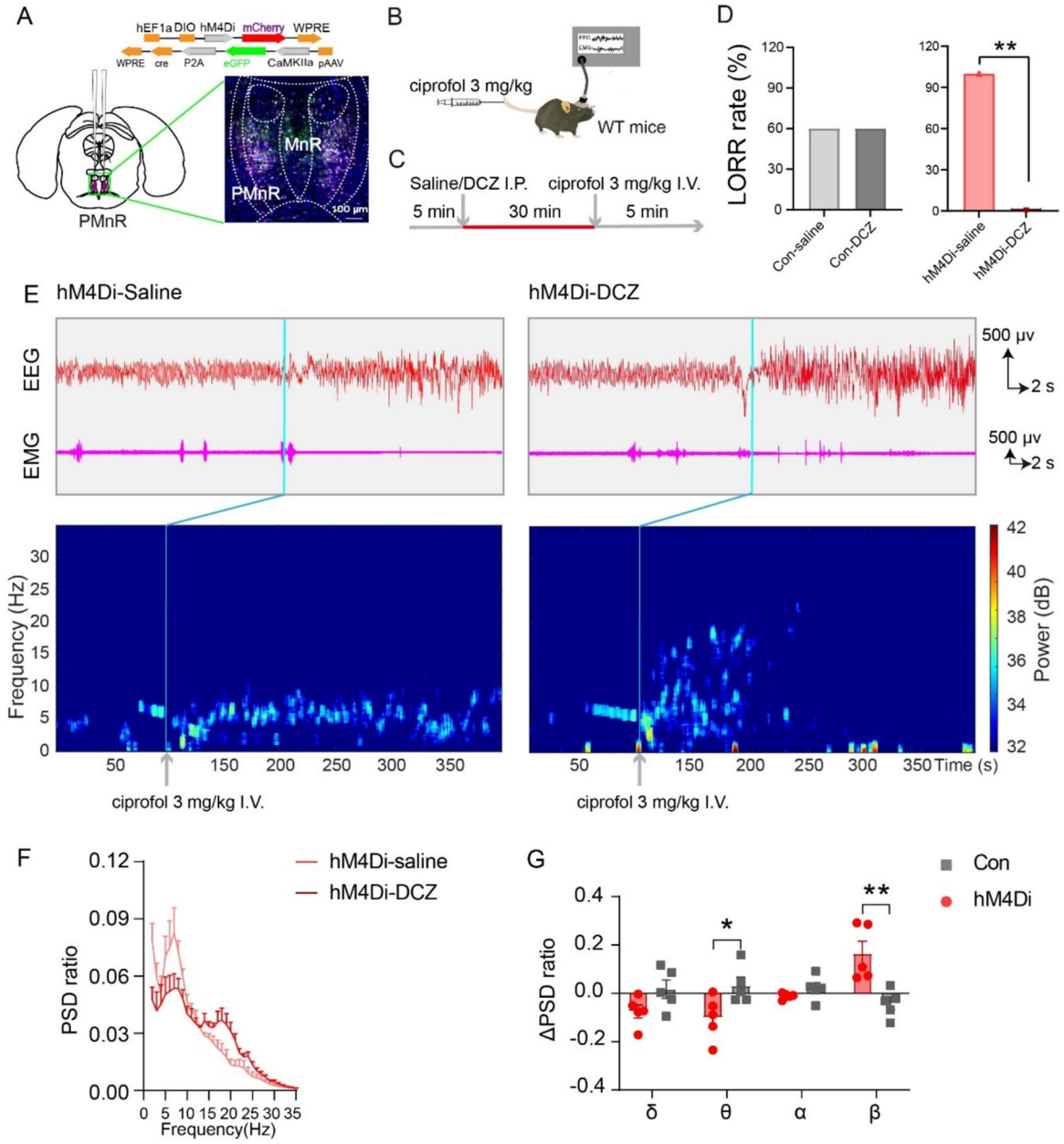

waves act as a hallmark of a lighter, earlier stage of GA, as chemogenetic inhibition decreased the θ wave power following pre-inhibition of the PMnR (Fig. 4).

It is widely recognized that propofol causes immobility by depressing the excitability of spinal neurons (Rudolph and Antkowiak 2004; Kubota et al. 2007; Grasshoff and Antkowiak 2004). In our study, mice had movement suppressed immediately by optogenetic activation of PMnR, implying that this state can be initiated from the brainstem and/or sequentially reinforced by the inhibition of the superficial sensory reflex arc in the spinal cord. It needs to be further distinguished whether the motionlessness is due to a lack of movement intention, motor nervous system inhibition, or the combined effect of the two.

In conclusion, our data reveal that the PMnR in the brainstem primarily consists of CaMKIIa$^+$ or VGAT$^+$ cells, commonly activated by propofol and ciprofol.

◂**Fig. 4** Chemogenetic inhibition of CaMKIIa$^+$ neurons in the PMnR region resist LORR and reduces the θ wave band. **A** Virus injection strategy and the representative coronal view of the injection site. **B** The layout of EEG and EMG recording, and experimental strategy for ciprofol injection and testing. **C** Experimental procedure and saline/DCZ administration. **D** LORR rate of DCZ treatment and saline treatment in control and hM4Di group ($n = 5$). **E** hM4Di group: Upper left: representative traces of EEG and EMG of the phase 20 s before and after 3 mg/kg ciprofol injection with saline treatment corresponding to the lower part. Upper right: representative traces of EEG and EMG of the phase 20 s before and after 3 mg/kg ciprofol injection with DCZ treatment corresponding to the lower part. Lower left: time–frequency spectrogram of EEG of the phase 100 s before and 300 s after 3 mg/kg ciprofol injection with saline treatment. Lower right: time–frequency spectrogram of EEG of the phase 100 s before and 300 s after 3 mg/kg ciprofol injection with DCZ treatment. **F** DCZ induced changes in the normalized global EEG wavelet PSD ratio from hm4di mice. Period included in data analysis: hM4Di-saline: phase from LORR mice unloaded from tail vein injection equipment to RORR; hM4Di-DCZ: 100-s period after unLORR mice unloaded from tail vein injector ($n = 5$). **G** PSD ratio changes of DCZ treatment compared with saline treatment in δ/θ/α/β ranges. (unpaired *t*-test: $t_\delta = 1.968$, $df = 4$; $t_\theta = 2.5070$, $df = 4$; $t_\alpha = 1.3550$, $df = 4$; $t_\beta = 3.6050$, $df = 4$). Two periods that interfere with EEG were removed when processing data: 1. the unstable period of recording EEG at the beginning; 2. the period of mice equipped with tail vein injection equipment. Also applicable to Fig. S6. Statistical analysis was performed using a paired *t*-test (parametric) in D and an unpaired *t*-test (parametric) in G. Data are presented as mean ± SEM. $^*p < 0.05$, $^{**}p < 0.01$, ns $p > 0.05$. Con, control group. See also Figure S6A. See also Video 3.1 and Video 3.2

Activation of PMnR CaMKIIa$^+$ neurons significantly promoted the transition from a state of wakefulness to anesthesia, as demonstrated by both behavioral observations and real-time EEG recordings. This finding identifies a novel node in the anesthetic network, enhancing our understanding of anesthesia efficacy. Our study offers valuable insights into the neural mechanisms underlying general anesthesia.

Acknowledgements We extend our gratitude to Chao Wei, Shilin Zhong, Heng Li, Zeyue Liu, Meizhu Huang, Li Zhang, Zhiyong Xie at the National Institute of Biological Sciences, Beijing, for brain stereotaxic injection technology, c-Fos staining, EEG technology, brain slice technique and Fos-CreER/+R26 Ai6/+ mice support and Xiaoqing Hao, Wanli Chen, Maohua Zhu, Zhengran Li at the Chinese Institute for Brain Research, Beijing, for technical support in animal experiments. Besides, special thanks to Chenyang Duan at the second hospital of Chongqing medical university for his invaluable support for this study. Additionally, we appreciate the insightful advice provided by Meimei Liao, Ran Huo, Keteng Lin, Hongxia Zhang, Xinyu Yang, Zhancong Xu, and Haijiao Zhao in E.E.Z.'s lab, which greatly contributed to the refinement of this article.

Author contributions Manuscript preparation: XHL and ZM; Methodology: XLL, CC, ZY and DS; Data analysis: TW, EEZ and GD; Conceptualization: XHL, ZM, DJ and HH. All authors approved the final version of the manuscript.

Funding This research was made possible through the generous support of the Ministry of Science and Technology of China (grant number 2021ZD0203400 awarded to E.E.Z.) and the National Natural Science Foundation of China (grant number 31971090 awarded to E.E.Z.). Their funding played a crucial role in facilitating the execution and completion of this study.

Data availability All data and materials in the article can be requested from the corresponding author.

Declarations

Ethics approval and consent to participate The Institutional Animal Care and Use Committee (IACUC) at the National Institute of Biological Sciences in Beijing (SYXK(京)2023-0007) approved all animal experiments.

Consent for publication Not applicable.

Competing interests The authors declare no competing interests.

References

Ao Y, Yang B, Zhang C, Wu B, Zhang X, Xing D, et al. Locus coeruleus to paraventricular thalamus projections facilitate emergence from isoflurane anesthesia in mice. Front Pharmacol. 2021;12:643172.

Arhem P, Klement G, Nilsson J. Mechanisms of anesthesia: towards integrating network, cellular, and molecular level modeling. Neuropsychopharmacology. 2003;28(Suppl 1):S40–7.

Bastos AM, Donoghue JA, Brincat SL, Mahnke M, Yanar J, Correa J, et al. Neural effects of propofol-induced unconsciousness and its reversal using thalamic stimulation. Elife. 2021;10:e60824.

Caggiano V, Leiras R, Goni-Erro H, Masini D, Bellardita C, Bouvier J, et al. Midbrain circuits that set locomotor speed and gait selection. Nature. 2018;553(7689):455–60.

Delorme A, Makeig S. EEGLAB: an open source toolbox for analysis of single-trial EEG dynamics including independent component analysis. J Neurosci Methods. 2004;134(1):9–21.

Esteves M, Almeida AM, Silva J, Silva Moreira P, Carvalho E, Pego JM, et al. MORPhA Scale: behavioral and electroencephalographic validation of a rodent anesthesia scale. J Neurosci Methods. 2019;324:108304.

Gelegen C, Miracca G, Ran MZ, Harding EC, Ye Z, Yu X, et al. Excitatory pathways from the lateral habenula enable propofol-induced sedation. Curr Biol. 2018;28(4):580-7 e5.

George Paxinos KBJF. The mouse brain in stereotaxic coordinates. secons edition ed. San Diego: Academic Press; 2001.

Gong X, Mendoza-Halliday D, Ting JT, Kaiser T, Sun X, Bastos AM, et al. An ultra-sensitive step-function opsin for minimally invasive optogenetic stimulation in mice and macaques. Neuron. 2020;107(1):38-51 e8.

Gordon-Fennell AG, Will RG, Ramachandra V, Gordon-Fennell L, Dominguez JM, Zahm DS, et al. The lateral preoptic area: a novel regulator of reward seeking and neuronal activity in the ventral tegmental area. Front Neurosci. 2019;13:1433.

Grasshoff C, Antkowiak B. Propofol and sevoflurane depress spinal neurons in vitro via different molecular targets. Anesthesiology. 2004;101(5):1167–76.

Guenthner CJ, Miyamichi K, Yang HH, Heller HC, Luo L. Permanent genetic access to transiently active neurons via TRAP: targeted recombination in active populations. Neuron. 2013;78(5):773–84.

Hagihara H, Shoji H, Otabi H, Toyoda A, Katoh K, Namihira M, et al. Protein lactylation induced by neural excitation. Cell Rep. 2021;37(2):109820.

Hagihira S. Changes in the electroencephalogram during anaesthesia and their physiological basis. Br J Anaesth. 2015;115(Suppl 1):i27–31.

Hagihira S. Brain mechanisms during course of anesthesia: what we know from EEG changes during induction and recovery. Front Syst Neurosci. 2017;11:39.

Hsu YW, Tempest L, Quina LA, Wei AD, Zeng H, Turner EE. Medial habenula output circuit mediated by alpha5 nicotinic receptor-expressing GABAergic neurons in the interpeduncular nucleus. J Neurosci. 2013;33(46):18022–35.

Jiang-Xie LF, Yin L, Zhao S, Prevosto V, Han BX, Dzirasa K, et al. A common neuroendocrine substrate for diverse general anesthetics and sleep. Neuron. 2019;102(5):1053-65 e4.

Ke R, Mignardi M, Pacureanu A, Svedlund J, Botling J, Wahlby C, et al. In situ sequencing for RNA analysis in preserved tissue and cells. Nat Methods. 2013;10(9):857–60.

Kubota I, Tsuboi Y, Shoda E, Kondo M, Masuda Y, Kitagawa J, et al. Modulation of neuronal activity in CNS pain pathways following propofol administration in rats: Fos and EEG analysis. Exp Brain Res. 2007;179(2):181–90.

Lanir-Azaria S, Meiri G, Avigdor T, Minert A, Devor M. Enhanced wakefulness following lesions of a mesopontine locus essential for the induction of general anesthesia. Behav Brain Res. 2018;341:198–211.

Lee M, Sanders RD, Yeom S-K, Won D-O, Seo K-S, Kim HJ, et al. Network properties in transitions of consciousness during propofol-induced sedation. Sci Rep. 2017;7(1):16791.

Leiras R, Cregg JM, Kiehn O. Brainstem circuits for locomotion. Annu Rev Neurosci. 2022;45:63–85.

Liao M, Gao X, Chen C, Li Q, Guo Q, Huang H, et al. Integrated neural tracing and in-situ barcoded sequencing reveals the logic of SCN efferent circuits in regulating circadian behaviors. Sci China Life Sci. 2023;67(3):518–28.

Lin J, Cheng X, Wang H, Du L, Li X, Zhao G, et al. Activation of astrocytes in the basal forebrain in mice facilitates isoflurane-induced loss of consciousness and prolongs recovery. BMC Anesthesiol. 2023;23(1):213.

Liu Y, Yu X, Zhu D, Zeng J, Lin Q, Zang B, et al. Safety and efficacy of ciprofol vs. propofol for sedation in intensive care unit patients with mechanical ventilation: a multicenter, open label, randomized, phase 2 trial. Chin Med J (Engl). 2022;135(9):1043–51.

Lu M, Liu J, Wu X, Zhang Z, Tokumine J. Ciprofol: a novel alternative to propofol in clinical intravenous anesthesia? BioMed Res Int. 2023;2023(1):7443226.

Ma Z, Eaton M, Liu Y, Zhang J, Chen X, Tu X, et al. Deficiency of autism-related Scn2a gene in mice disrupts sleep patterns and circadian rhythms. Neurobiol Dis. 2022;168:105690.

Madisen L, Zwingman TA, Sunkin SM, Oh SW, Zariwala HA, Gu H, et al. A robust and high-throughput Cre reporting and characterization system for the whole mouse brain. Nat Neurosci. 2010;13(1):133–40.

Moody OA, Zhang ER, Vincent KF, Kato R, Melonakos ED, Nehs CJ, et al. The neural circuits underlying general anesthesia and sleep. Anesth Analg. 2021;132(5):1254–64.

Nagai Y, Miyakawa N, Takuwa H, Hori Y, Oyama K, Ji B, et al. Deschloroclozapine, a potent and selective chemogenetic actuator enables rapid neuronal and behavioral modulations in mice and monkeys. Nat Neurosci. 2020;23(9):1157–67.

Nelson LE, Guo TZ, Lu J, Saper CB, Franks NP, Maze M. The sedative component of anesthesia is mediated by GABA(A) receptors in an endogenous sleep pathway. Nat Neurosci. 2002;5(10):979–84.

Prerau MJ, Brown RE, Bianchi MT, Ellenbogen JM, Purdon PL. Sleep neurophysiological dynamics through the lens of multitaper spectral analysis. Physiology (Bethesda). 2017;32(1):60–92.

Qin L, Ren L, Wan S, Liu G, Luo X, Liu Z, et al. Design, synthesis, and evaluation of novel 2,6-disubstituted phenol derivatives as general anesthetics. J Med Chem. 2017;60(9):3606–17.

Root DH, Zhang S, Barker DJ, Miranda-Barrientos J, Liu B, Wang HL, et al. Selective brain distribution and distinctive

synaptic architecture of dual glutamatergic-GABAergic neurons. Cell Rep. 2018;23(12):3465–79.
Rudolph U, Antkowiak B. Molecular and neuronal substrates for general anaesthetics. Nat Rev Neurosci. 2004;5(9):709–20.
Sakurai T, Nagata R, Yamanaka A, Kawamura H, Tsujino N, Muraki Y, et al. Input of orexin/hypocretin neurons revealed by a genetically encoded tracer in mice. Neuron. 2005;46(2):297–308.
Sang D, Lin K, Yang Y, Ran G, Li B, Chen C, et al. Prolonged sleep deprivation induces a cytokine-storm-like syndrome in mammals. Cell. 2023;186(25):5500-16.e21.
Singh K, Cauzzo S, Garcia-Gomar MG, Stauder M, Vanello N, Passino C, et al. Functional connectome of arousal and motor brainstem nuclei in living humans by 7 Tesla resting-state fMRI. Neuroimage. 2022;249:118865.
Sos KE, Mayer MI, Cserep C, Takacs FS, Szonyi A, Freund TF, et al. Cellular architecture and transmitter phenotypes of neurons of the mouse median raphe region. Brain Struct Funct. 2017;222(1):287–99.
Stringer C, Wang T, Michaelos M, Pachitariu M. Cellpose: a generalist algorithm for cellular segmentation. Nat Methods. 2021;18(1):100–6.
Tian F, Lewis LD, Zhou DW, Balanza GA, Paulk AC, Zelmann R, et al. Characterizing brain dynamics during ketamine-induced dissociation and subsequent interactions with propofol using human intracranial neurophysiology. Nat Commun. 2023;14(1):1748.
Wang D, Guo Y, Li H, Li J, Ran M, Guo J, et al. Selective optogenetic activation of orexinergic terminals in the basal forebrain and locus coeruleus promotes emergence from isoflurane anaesthesia in rats. Br J Anaesth. 2021;126(1):279–92.
Wang YW, Hu Y, Qi JT, Zhang Z, Luo MQ. Comparative whole-brain mapping of isoflurane and ketamine-activated nuclei and functional networks. eLife. 2023. https://doi.org/10.7554/eLife.88420.1.
Wasilczuk AZ, Maier KL, Kelz MB. The mouse as a model organism for assessing anesthetic sensitivity. Methods Enzymol. 2018;602:211–28 (Chemical and biochemical approaches for the study of anesthetic function, part A).
Xia J-M, Fan B-Q, Yi X-W, Ni W-W, Zhou Y, Chen D-D, et al. Medial septal glutamatergic neurons modulate states of consciousness during sevoflurane anesthesia in mice. Anesthesiology. 2023;140(1):102–15.
Xu L, Liu M-Z, Yang Y-Y, Wang Y, Hua X-X, Du L-X, et al. Geraniol enhances inhibitory inputs to the paraventricular thalamic nucleus and induces sedation in mice. Phytomedicine. 2022;98:153965.
Yi T, Wang N, Huang J, Wang Y, Ren S, Hu Y, et al. A sleep-specific midbrain target for sevoflurane anesthesia. Adv Sci (Weinh). 2023;10(15):e2300189.
Zhang D, Liu J, Zhu T, Zhou C. Identifying c-fos expression as a strategy to investigate the actions of general anesthetics on the central nervous system. Curr Neuropharmacol. 2022;20(1):55–71.
Zhou X, Li A, Mi X, Li Y, Ding Z, An M, et al. Hyperexcited limbic neurons represent sexual satiety and reduce mating motivation. Science. 2023;379(6634):820–5.